Effect of aromatic fuels and premixing on aromatic species and soot distributions in laminar, co-flow flames at atmospheric pressure

*A. Makwana, S. Iyer, M. Linevsky, R. Santoro, T. Litzinger, J. O'Connor**

Department of Mechanical Engineering, The Pennsylvania State University, UP, PA, USA

*Corresponding Author: Jacqueline O'Connor

111 Research East Building, University Park, PA, 16802

814.863.1502, jxo22@engr.psu.edu

Abstract: The aim of the present study is to investigate the effects of aromatic fuel structure on the aromatic species and the soot volume fraction in laminar, co-flow flames at atmospheric pressure. Both non-premixed and partially-premixed flames (jet equivalence ratios of 24 and 6) are studied. The four fuels consist of binary mixtures of *n*-dodecane with one of four aromatic species: *n*-propylbenzene, toluene, *m*-xylene, and 1,3,5-trimethylbenzene. For all flame conditions, the total carbon flow rate of the fuel mixture is kept constant. Furthermore, in each binary mixture, the carbon mole fraction from the *n*-dodecane and the aromatic component is kept constant. Laser-induced incandescence (LII) and laser extinction are used to obtain two-dimensional soot volume fraction in the flames. Laser-induced fluorescence (LIF) is used to obtain the two-dimensional aromatic species distribution in the flames. The experimental results indicate that the 1,3,5-trimethylbenzene/*n*-dodecane flame has the highest peak soot volume fraction amongst the four fuels; the other three fuel mixtures, within measurement uncertainty, have similar peak soot volume fraction. Additionally, premixing changes the spatial distribution of polycyclic aromatic hydrocarbons and soot in the flames. In the non-premixed cases, the peak soot volume fraction is located in an annular region near the flame sheet, whereas the soot field is more uniform across the cross-section of the flame at a jet equivalence ratio of 6. A published aromatic fuel chemical mechanism is used to understand the differences in the pathways to soot precursors among the aromatic fuels. The combined 2D LIF and LII result provide a unique dataset to validate

soot and chemical numerical models for the four aromatic fuels: *n*-propylbenzene, toluene, *m*-xylene, and 1,3,5-trimethylbenzene.

Keywords: *n*-propylbenzene, toluene, *m*-xylene, 1,3,5-trimethylbenzene, soot volume fraction

Nomenclature

Symbol	Name
2-D	Two dimensional
C12	Pure *n*-dodecane
HAB	Height above the burner
LE	Laser extinction
LIF	Laser induced fluorescence
LII	Laser induced incandescence
mX	*m*-xylene/*n*-dodecane mixture
N_2	Nitrogen
PAH	Polycyclic aromatic hydrocarbons
PB	*n*-propylbenzene /*n*-dodecane mixture
TMB	1,3,5-trimethylbenzene/*n*-dodecane mixture
TOL	toluene/*n*-dodecane mixture
TSI	Threshold soot index
f_v	Soot volume fraction
ϕ_{jet}	Jet equivalence ratio

1. Introduction

Conventional jet fuels are typically composed of four main classes of molecules: *n*-paraffins, *iso*-paraffins, cycloparaffins, and aromatics [1]. Aromatic molecules form a significant fraction of the total volume of hydrocarbons present in diesel and gasoline fuels as well [2, 3]. These aromatic molecules produce substantially higher soot as compared to the aliphatic hydrocarbons because of their role in the formation of soot precursors, polycyclic aromatic hydrocarbons (PAH) of molecular weight 500-1000 amu [4]. In this study, we consider the impact of aromatic structure on soot processes in laminar co-flow flames through the addition of *n*-propylbenzene, toluene, *m*-xylene, and 1,3,5-trimethylbenzene to *n*-dodecane.

Zhang *et al*. [5] studied the effect of addition of *n*-propylbenzene and *n*-dodecane on soot volume fraction (f_v), primary particle diameter, and number density in a methane laminar co-flow non-premixed flame. Three different fuel mixtures of *n*-propylbenzene and *n*-dodecane were studied by keeping inlet carbon flow rate constant. The mole fraction of the *n*-propylbenzene and *n*-dodecane was 3% of the total fuel flow rate. Zhang *et al.* [5] found that the effect of aromatic chemistry was found to be stronger along the centerline, as the aromatic component increased both the soot inception and surface growth processes. In the annular region of the flame, the aromatic component influenced only the soot inception process by providing a higher population of soot incipient particles. Moss and Aksit [6] reported the f_v measurement using laser extinction, temperature using thermocouples, and mixture fraction measurements using mass spectroscopy for a binary mixture of 77% by volume *n*-decane and 23% by volume 1,3,5-trimethylbenzene in a diffusion flame. They also developed a flamelet-based two-equation model to predict soot. The study reported that the soot model with a surface growth mechanism involving benzene and one without benzene as the contributing species, albeit different scaling parameters, yielded similar soot volume fractions.

Conturso *et al*. [7] studied the sooting tendency of *n*-propylbenzene, *iso*-propylbenzene, and 1,3,5-trimethylbenzene in a counter-flow ethylene diffusion flame. The fuel stream of ethylene was doped with 10%, 20%, and 30% of total carbon with the aromatic fuels. They compared the results with toluene and xylene fuels from their companion study [8]. They found that *iso*-propylbenzene had a higher tendency of particulate formation as compared to the *n*-propylbenzene; this observation was contradictory to the earlier studies [9, 10] of sooting tendency of aromatic

molecules. The authors' concluded that the differences in their study could be a result of flame configuration, counterflow versus co-flow. Secondly, the level of the second fuel level in their study was 20% of total carbon flow rate, which could change the flame structure; the previous work [9, 10] used small amounts, 2-500 ppm, of dopants. Furthermore, the study reported that increasing the number of methyl groups on the aromatic ring didn't have an effect on the sooting tendency of the fuels. They found toluene, the three xylenes, and 1,3,5-trimethylbenzene had similar sooting tendencies.

In addition to non-premixed flames, partially-premixed flames are of practical importance in gas turbine engines, where fuel and air first mix in the primary zone of the combustor. Harris and Weiner [11] studied soot particle growth in ethylene and ethylene/toluene flame in premixed flat flames. They found that for a particular C/O ratio, the soot inception was higher in toluene/ethylene flames as compared to ethylene flames. However, the rate of surface growth per unit area was higher in the ethylene flame as compared to the toluene/ethylene flame due to higher concentration of acetylene in the ethylene flame. D'Anna *et al*. [12] characterized the chemistry of *n*-heptane (C/O=0.7 and 0.8) and 90 vol% *n*-heptane/10% vol *n*-propylbenzene (C/O=0.8) in a McKenna burner. The addition of *n*-propylbenzene to *n*-heptane resulted in the increase in benzene and PAH concentration, which resulted in earlier occurrence of and increased levels of soot inception in an *n*-propylbenzene/*n*-heptane flame as compared to an *n*-heptane flame. However, the final soot loading was found to be similar in both the *n*-propylbenzene/*n*-heptane and *n*-heptane flames. Modelling by these same authors found that in the *n*-heptane flame, the larger contribution of soot mass growth, due to slightly higher temperature and earlier, larger presence of acetylene, counterbalanced the higher soot inception in the *n*-propylbenzene/*n*-heptane flame.

These previous studies show that the effect of an aromatic fuel on soot loading depends on the flame conditions, which drive the soot inception and growth processes. Furthermore, the premixed flame studies [13-16] indicate that premixing can change the distribution of the intermediate products formed from fuel decomposition. This change in intermediate products can result in either an increase or decrease of soot emission, depending on the fuel type and level of premixing. These points highlight the need to systematically investigate the effect of premixing on soot precursors and soot under similar flame conditions to that of non-premixed flames. The aim of the present work is to investigate the effect of single-ring aromatic fuel structure on the distribution of the aromatics and soot in a co-flow flame at atmospheric pressure. In particular, we consider mixtures

that better represent real fuels, where a carrier gas of nitrogen, instead of light hydrocarbons, is used to convect pre-vaporized aromatic and *n*-dodecane mixtures. In studies involving methane or ethane as a carrier gas, the chemistry of the carrier gas can have an impact on the sooting tendency of the fuel. In the current study, the absence of methane or ethane as a carrier gas helps to isolate the effects of the chemistry of the real fuels on the soot, making these results more representative of fuel mixtures in engine applications.

The four single-ring aromatic fuels investigated in this study are *n*-propylbenzene, toluene, *m*-xylene, and 1,3,5-trimethylbenzene. In choosing these fuels, we are interested in the effects of the number of methyl groups and the lengthening of the aliphatic chain on the aromatic ring. In addition, these four aromatic fuels are important fuel surrogate components [17, 18]. The alkyl benzenes on average form 13.4% volume fraction of jet fuels, and 1,3,5-trimethylbenzene is considered an important component for tuning the extinction and ignition limits in the formulation of a surrogate fuel [18]. These four molecules have been used in a number of surrogate fuel studies [17, 19, 20]. Furthermore, 1,3,5-trimethylbenzene forms a significant volume fraction in two category-C test fuels, and surrogate fuels S-1 and S-2, in the National Jet Fuels Combustion Program [21].

In addition, we investigate the effect of premixing on aromatics and soot at two different jet equivalence ratios (ϕ_{jet}) of 24 and 6. To the best of the authors' knowledge, no study has reported two-dimensional results of both aromatic species and soot volume fraction for these four aromatic fuels in both non-premixed and premixed co-flow flames under similar burner conditions. This work advances our findings from Yefu *et al*. [22] and Makwana *et al*. [23], where we investigated the effect of *n*-alkane, *iso*-alkane, cycloalkane, and one aromatic fuels on the distribution of aromatics and soot. The combined laser induced incandescence (LII) - laser induced fluorescence (LIF) experimental results presented here can be used to validate numerical models for the four aromatic molecules.

2. Methods/Experiment

The fuel test matrix is investigated in a modified version of the laminar, co-flow burner used by Santoro *et al.* [24]. The burner is modified in order to operate with high molecular weight fuels. The detailed design of the burner and the burner system are discussed in Ref. [22, 23]. The burner

consists of two concentric brass tubes; the inner and outer tube diameter are 0.436 in. and 4 in. diameter, respectively. The inner fuel tube is 0.157 in. above the exit plane of the co-flow air.

In the current study, we use laser induced incandescence (LII) and laser extinction (LE) to obtain two-dimensional (2-D) soot volume fractions in the flame. Laser-induced fluorescence (LIF) is used to obtain 2-D aromatics distributions in the flame. We classify aromatic molecules in two groups: one and two ring aromatics and three to five ring aromatics, by collecting the LIF signal over two different wavelength ranges. The details of the filters is provided in Wang *et al.* [22]. The temperature measurements are obtained using R-type thermocouples. The temperature measurements have been corrected for radiation losses by using approach similar to that described in Ref. [22]. The setup, data collection and analysis, and measurement uncertainties for LII, LIF, LE, and temperature measurement used in this study is identical to those described in Ref. [22]. A value of $\tilde{m} = 1.57 - 0.56i$ is used as the refractive index of soot to be consistent with previously published work [25]. A calibration factor of 3350 LII counts corresponds to 1 ppm of soot [22]. The estimated uncertainty in the f_v measurement through laser extinction and calibration of LII data is ±15%. In aromatic flames, the LII signal from the centerline has an additional uncertainty of 30-35% on account of LII signal trapping [26]. In LE, the choice of refractive index of soot can result in further uncertainties in f_v [27]. Further details of the experiment and diagnostics are provided in Appendix B of the Supplemental Material.

Fuel matrix.

The fuel matrix is comprised of four binary fuel mixtures of *n*-dodecane with *n*-propylbenzene, toluene, *m*-xylene, and 1,3,5-trimethylbenzene. The *n*-dodecane fuel used in this study is meant to represent the *n*-alkane class in a real fuel [18]. A significant volume fraction of conventional fuels is comprised of *n*-alkanes, and hence, the decomposition of the *n*-dodecane builds a radical pool similar to that in real fuels. The use of binary mixtures also helps to retain similar thermal conditions in the fuel decomposition region, and therefore, isolates the chemical effect of the aromatic fuel.

The fuel mixtures and some of their properties are outlined in Table 1. In addition to these four fuel mixtures, results of *n*-dodecane are provided from Ref. [22, 23] to illustrate the effect of adding different aromatic fuels to *n*-dodecane on the aromatic species and soot distribution in the flames. The results for *m*-xylene are obtained from Refs. [22, 23]. Additionally, results of

premixing on peak f_v at higher nitrogen dilution in the *m*-xylene fuel are reported here, which were not discussed in Refs. [22, 23]. The liquid volume fraction of *m*-xylene in the *m*-xylene/*n*-dodecane mixture was set at 25%. According to the ASTM D1319 specification, 25% is the maximum allowable volume fraction of aromatics in JP-8 [28]. For the other three binary fuel mixtures, the liquid volume fraction of the aromatic fuel is determined such that the percentage of carbon coming each of the two components of the binary mixture is constant. The total carbon flow rate is held constant at 0.0111 mole/min. All of the hydrocarbons used in this study have purity greater than 98.5%.

Table 1: Matrix of binary fuel mixtures; major component in mixtures is *n*-dodecane.

Fuel mixture Second component	Liquid Fuel flow rate (ml/min)	Liquid Volume fraction (%)	Carbon mole fraction	Mole fraction (%)	Co-flow air flow rate (scfm)	MW (g/mol)	H/C ratio
n-propylbenzene (PB)	0.2004	25.1	0.292	35.4	4	120	1.92
toluene (TOL)	0.1995	24.8	0.292	41.3	4	92	1.87
m-xylene (mX)	0.2000	25.0	0.292	38.2	4	106	1.90
1,3,5-trimethylbenzene (TMB)	0.2003	25.1	0.292	35.4	4	120	1.92

3. Results and Discussion

The visible flame images of the five fuels (not shown) obtained using a digital camera at the same camera operating parameters show that the aromatic flame heights are similar at ϕ_{jet} = Inf and ϕ_{jet} = 6. At ϕ_{jet} = Inf conditions, the four aromatic flames are smoking such that the tip is open and not all the soot is oxidized; all tips close at ϕ_{jet} = 6. These results are discussed in Appendix C.

3.1 Comparison of the temperature field

Figure 1 shows the radial (at 5 mm HAB) and centerline (until 20 mm HAB) temperature profiles for the five fuels at the non-premixed condition. While no soot deposition on the thermocouple bead is observed at distances upstream of 20 mm HAB, soot deposition downstream of this location affects temperature measurements; therefore, we do not report temperature beyond this point. The trend in centerline and radial temperature profiles is identical to previous work [22, 23] . For the five fuels, Fig. 1 shows that the temperature field is similar, within the measurement uncertainty of ± 100K. The uncertainty in spatial location of thermocouple bead is estimated to be ± 0.5 mm. However, the temperature field downstream of 20 mm HAB is expected to be different on account of different levels of soot amongst the five fuels [29]. The radial temperature measurement at 5 mm HAB and along the flame centerline until 18 mm HAB in the $\phi_{jet} = 6$ flames, provided in Appendix D of the Supplementary Material, show similar trends as the non-premixed flames. The five fuels have similar temperatures in the fuel pyrolysis zone at each ϕ_{jet}.

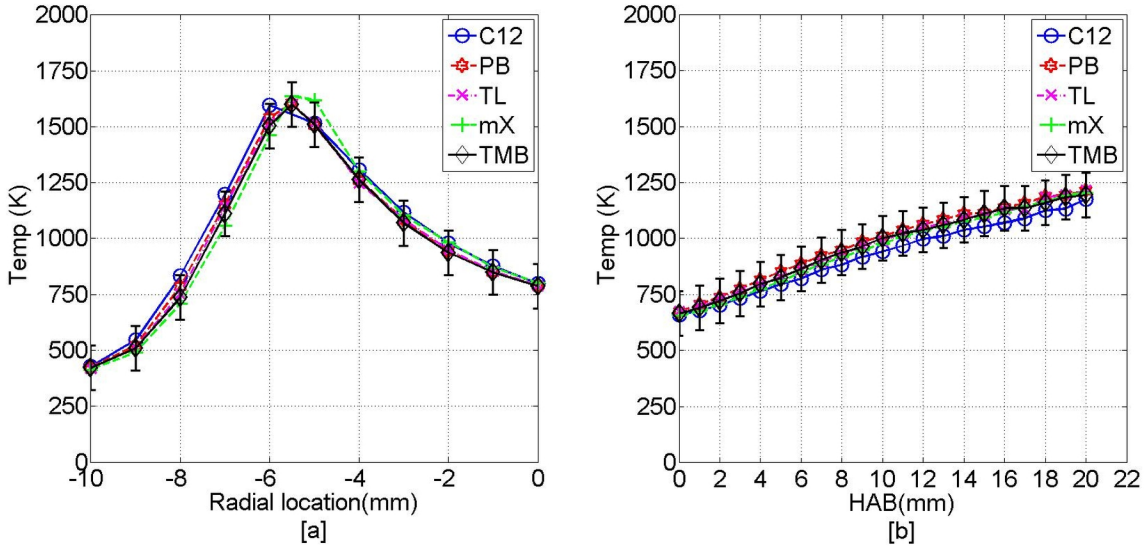

Figure 1. Corrected temperature measurement for ϕ_{jet} = Inf flame: (a) Radial at 5 mm HAB; (b) Centerline until 20 mm HAB.

3.2 Small and large aromatics spatial distribution.

The similarity in the temperature field in the fuel pyrolysis zone among the five fuels and the similar boundary conditions at a particular ϕ_{jet} indicate that the differences visible in the small and large aromatics amongst the five fuels are likely due to chemical, not thermal, effects. The

pyrolysis of the four aromatic fuel mixtures is studied using numerical simulation in a homogenous reactor at constant temperature (1600 K) and pressure (1 atm) to compare the initial pathways of fuel consumption for the four fuels. The published aromatic fuels chemistry from Malewicki *et al*. [30] is used for these simulations. The details of the numerical simulation are provided in Appendix E of the Supplementary Material.

The numerical simulation shows that, initially, *n*-propylbenzene can form benzyl radicals by C-C bond fission due to thermal decomposition. Furthermore, once chain-carrying radicals are available from *n*-dodecane decomposition, *n*-propylbenzene can also undergo H-abstraction by H or CH_3 radicals to form 1-phenyl-1-propyl radical, which subsequently forms styrene. Additionally, *n*-propylbenzene can undergo H-abstraction by H radicals to form 1-phenyl-2-propyl and 3-phenyl-1-propyl radicals that can consequently form C6H5C3H5-2 and benzyl radicals, respectively. The toluene mixture pyrolysis demonstrates that toluene is primarily consumed by C-H bond fission or H-abstraction by H radical to form benzyl radical. Additionally, the simulation shows that toluene can also react with H radicals to form $C_6H_6CH_3$ or benzene and a methyl radical. The comparison of the normalized mole fraction of toluene and *n*-propylbenzene shows that the consumption of *n*-propylbenzene is faster than that of toluene. The relative trend of consumption of the two fuels is consistent with previous work involving *n*-propylbenzene and toluene [31]; the weaker C-C bond in *n*-propylbenzene as compared to the C-H bond in the methyl side chain in toluene results in faster consumption of *n*-propylbenzene.

The *m*-xylene fuel mixture pyrolysis simulation shows that *m*-xylene primarily forms *m*-xylyl radical by C-H fission. Once *n*-dodecane undergoes decomposition, *m*-xylene undergoes H abstraction by the CH_3 or H radical to form *m*-xylyl. The 1,3,5-trimethylbenzene fuel simulation demonstrates that it forms C_9H_{11} by C-H bond fission from the methyl side chain, or H-abstraction by H or CH_3 radicals. 1,3,5-trimethylbenzene can also react with a H radical to form *m*-xylene and a CH_3 radical. These simulations show that the four aromatic fuels are consumed through different reaction pathways at different rates, which result in differences in the initial pool of aromatic radicals.

In the present study, the aromatics-LIF signal collected in each wavelength band, for small and large aromatics [22], is emitted from a number of different species. The previous work involving fluorescence of aromatic species showed that different aromatic molecules can have significantly

different absorption cross-sections and fluorescence quantum yields [32, 33]. Due to the differences in the initial pool of aromatic radicals formed from the parent aromatic fuels, combined with incomplete knowledge of the effects of temperature on fluorescence quantum yield and absorption cross-section for the aromatic species, we are unable to calibrate the aromatic-LIF signal to obtain quantitative information about the gas phase species. Therefore, small and large aromatic results are presented on a normalized scale of 0-1, where each data set is normalized by the corresponding peak value of the LIF signal. If the peak LIF signal is located at the tube exit due to excitation of the fuel molecules, the peak LIF signal from the downstream location is selected as the value to normalize the data set. Therefore, the primary information gained from the aromatic-LIF measurement is the spatial development of aromatics and how this spatial distribution changes with fuel molecular structure. Moreover, the LIF measurements provide information about the effect of premixing the fuel jet on the spatial distribution of aromatics, which in turn can affect soot inception and soot growth through PAH condensation.

Figure 2 shows the 2-D spatial distribution of small aromatics for the five fuels, each presented on a normalized scale of zero to one. Therefore, the data can only be viewed qualitatively, not quantitatively. An iso-contour of 20% of the peak LIF signal of the *n*-dodecane flame, equivalent to 4200 counts, is shown on all the 2D LIF-images to illustrate the spatial extent of the LIF signal. Figure 2 shows that the signal strength is higher on the left side of the image as compared to the right side of the image. This LIF-signal intensity difference on left and right half of the flame is caused by laser fluence attenuation due to absorption by PAHs as the laser beam traverses through the flame from the left to the right side of the image. Figure 2 (b)-(e) shows the presence of LIF signal at the tube exit, although the intensity of the LIF signal for the four flames is different. The LIF signal is present at the tube exit because the fuel molecules, *n*-propylbenzene, toluene, *m*-xylene, and 1,3,5-trimethylbenzene, are themselves single-ring aromatic species, and they fluoresce in the wavelength band in which the small aromatics LIF signal is collected. Furthermore, Fig. 1 (b) shows the temperature at the tube exit is similar, 700 K, for all the flames. Therefore, the difference in the intensity of LIF signal in the four aromatic flames at the tube exit is likely due to differences in the mole fraction of the aromatic species and their absorption coefficient at 266 nm [33].

A comparison of the spatial distribution of small aromatics in the *n*-dodecane flame, in Fig. 2 (a), relative to that in the four aromatic flames, in Fig. 2 (b)-(e), shows that the presence of an

aromatic component in the fuel changes the spatial extent of the small aromatics for the four aromatic flames as compared to the *n*-dodecane flame. Furthermore, beyond the cone region at the tube exit, the 2-D small aromatics LIF structure is quite similar; the peak LIF signal occurs in the annular region at 5-10 mm HAB in the aromatic fuels and at 10-20 mm HAB in the *n*-dodecane flame. The higher LIF signal intensity at lower HAB in the aromatic flames as compared to the *n*-dodecane fuel is due to the accelerated path to the formation of one and two ring aromatics from a fuel that contains one ring aromatics. Previous studies involving *m*-xylene [34, 35], *n*-propylbenzene [10, 36, 37], 1,3,5-trimethylbenzene [38, 39], and toluene [10, 40, 41] have shown direct pathways to polycyclic aromatic hydrocarbons from the initial fuel ring.

The comparison of the small aromatics for the four aromatics fuels, Fig. 2 (b)-(e), shows that the spatial distribution of small aromatics is similar for the four aromatic fuels. Downstream of the LIF signal from fuel florescence, the LIF signal intensity decreases. The initial decrease in the LIF signal is due to the decrease in the mole fraction of the aromatic fuel, since the total number of moles increases as a result of the *n*-dodecane decomposition. Furthermore, the diffusion of the aromatic fuel and formation of new aromatic species with different quantum yields as compared to the parent fuel may also result in the initial decrease in the LIF signal.

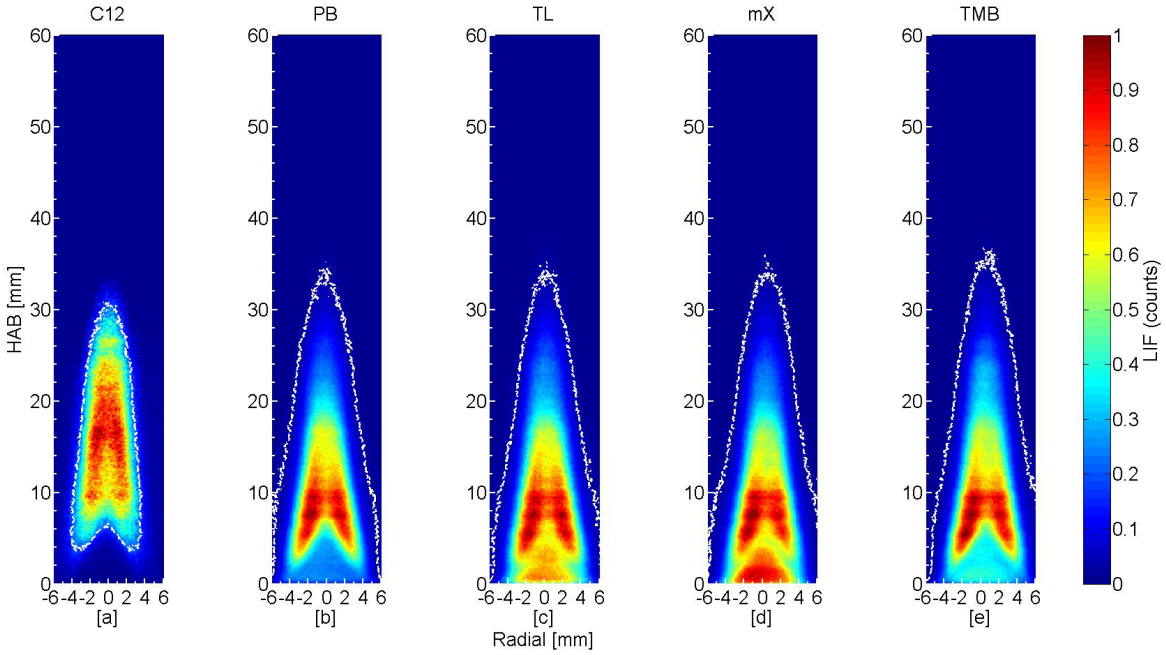

Figure 2. Two dimensional LIF image for small aromatics [normalized counts] for ϕ_{jet} = Inf: (a) *n*-dodecane flame; (b) *n*-propylbenzene flame; (c) toluene flame; (d) *m*-xylene flame; (e) 1,3,5-trimethylbenzene flame.

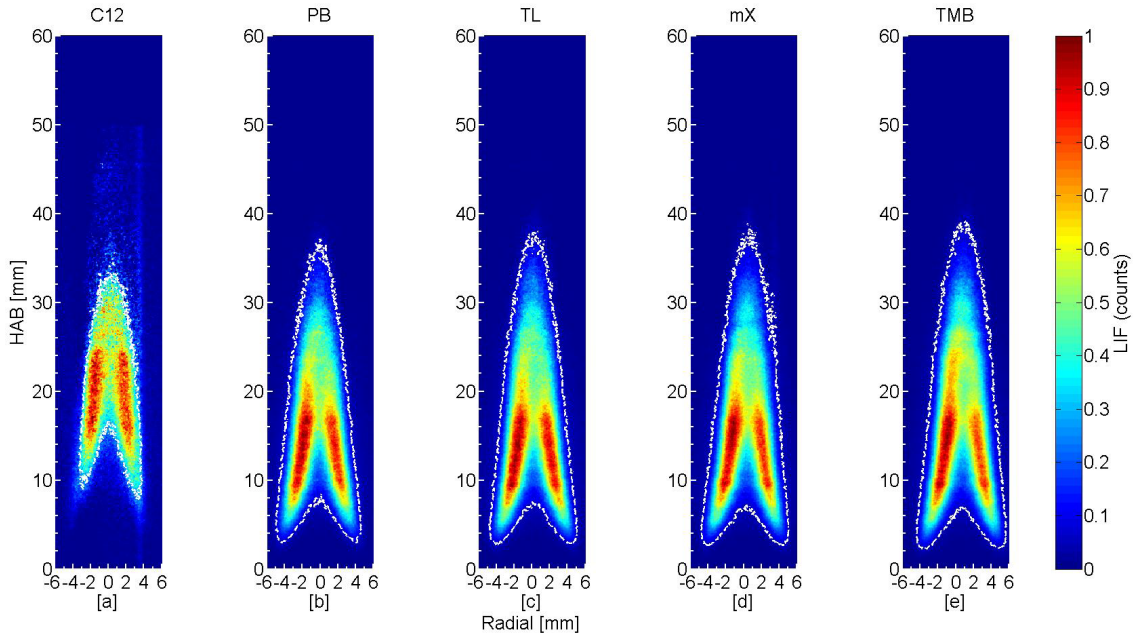

Figure 3. Two dimensional LIF image for large aromatics [normalized counts] for ϕ_{jet} = Inf: (a) *n*-dodecane flame; (b) *n*-propylbenzene flame; (c) toluene flame; (d) *m*-xylene flame; (e) 1,3,5-trimethylbenzene flame.

Further downstream, the LIF signal increases as new one and two ring aromatics are formed. Comparison of the trend of the LIF signal from the *n*-dodecane and aromatic fuels on the centerline streamline shows that in the aromatic fuels, the LIF signal starts to increase at approximately 5 mm HAB; this HAB is similar to the height above the tube exit where the LIF signal is first detected in the *n*-dodecane flame. Therefore, the increase in LIF signal in the aromatic fuels is likely because of formation of one and two ring species from the decomposition products of *n*-dodecane. The radicals from *n*-dodecane decomposition may contribute to the growth of other one and two ring aromatics from one ring radicals like benzyl, *m*-xylyl, styrene, and others, which are formed from parent aromatic fuels. Further downstream, the LIF signal decreases again as these small aromatics form larger PAHs, are oxidized, or are consumed via soot growth.

The large aromatics are shown in Fig. 3; each of the five figures have been normalized by the corresponding peak value of the LIF signal and all use a normalized color scale of zero to one. The

five figures can only be compared qualitatively. The 2-D spatial distribution of large aromatics for the *n*-dodecane flame and the four aromatic flames is similar, although the large aromatics in the *n*-dodecane flame are shifted downstream from those in the aromatic-fueled flames; the peak LIF signal intensity occurs in the flame annular region as compared to on the flame centerline for all five fuels. In spite of the similarities in the 2-D structure between the *n*-dodecane and four aromatic flames, there are some differences that are evident from Fig. 3. In aromatic fuels, the LIF signal is detected over a larger spatial extent, from approximately 3 mm to 40 mm HAB, as compared to 8 mm to 35 mm HAB for the *n*-dodecane flame. The earlier detection of large aromatics LIF signal in a flame with an aromatic fuel component as compared to the *n*-dodecane flame is expected, as the aromatic fuels contain a single ring aromatic, and so the growth to large PAHs is accelerated. Along the centerline streamline, the LIF signal increases first due to dominant PAH formation processes and then decreases at further downstream locations as aromatics are oxidized, form larger PAH, or contribute to soot growth through PAH condensation.

At the partially-premixed condition, the small and large aromatics 2-D spatial distribution for the $\phi_{jet} = 6$ flames are presented in Fig. 4. The LIF signals from the flames presented in Fig. 4 have been normalized by the corresponding peak value. Similar to the aromatic distribution in the non-premixed flames, the small aromatic distribution is similar for the four aromatics fuels in the premixed flames, and therefore, only results from the 1,3,5-trimethylbenzene/*n*-dodecane flame are presented here; the remainder of the results are shown in the Supplemental Material. A comparison of the small aromatics of the *n*-dodecane flame, in Fig. 4 (a), to the aromatics flame shown in Fig. 4 (b), shows that addition of an aromatic component to *n*-dodecane results in a change in the spatial distribution of small aromatics. The *n*-dodecane flame has peak LIF signal in a region close to the flame centerline at 20-25 mm HAB. However, the aromatic fuel has a peak LIF signal in the flame annular region between 7 mm and 22 mm HAB.

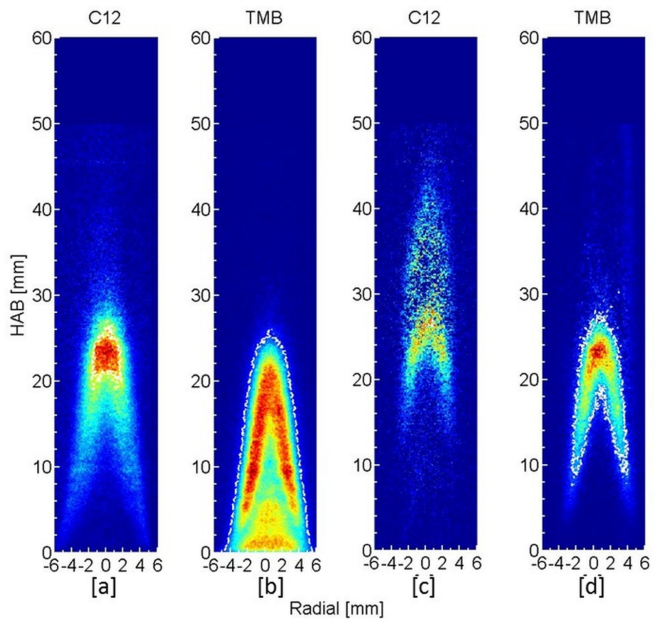

Figure 4. Two dimensional LIF image for aromatics [Normalized counts] for $\phi_{jet} = 6$: (a) Small aromatics, *n*-dodecane flame; (b) Small aromatics,1,3,5-trimethylbenzene flame; (c) Large aromatics, *n*-dodecane flame; (d) Large aromatics,1,3,5-trimethylbenzene flame.

The large aromatic spatial distribution for the *n*-dodecane, $\phi_{jet} = 6$ flame shown in Fig. 4 (c) has a low signal-to-noise ratio due to decreasing concentration of large aromatics; the LIF signal is comparable to the noise at 30-40 mm HAB. A comparison of the large aromatics in the aromatic fuel in Fig. 4 (d) and *n*-dodecane fuel in Fig. 4 (c) shows that the spatial distribution is similar, in spite of the differences in the small aromatics. The peak LIF signal is located near the flame centerline at 20-25 mm HAB.

The discussion until now has focused on the effects of the addition of aromatic fuels and premixing on the spatial development of the aromatic species, which provide important information on the distribution of gas-phase species. The 2-D spatial distribution of the small and large aromatics amongst the four aromatic fuels, within the measurement uncertainty, is quite similar at a particular ϕ_{jet}. Furthermore, premixing the fuel jet results in substantial changes in the 2-D spatial distribution of the aromatic-LIF measurements in the aromatic fuels. The peak LIF intensity of small and large aromatics decreases as a result of premixing. Additionally, the first location of detection of large aromatics shifts to higher HAB due to premixing. The decrease and shift in first location of detection of large aromatics to higher HAB due to premixing is likely the result of a combination of chemical, dilution, and thermal effects, which are discussed in detail in Makwana *et al*. [23].

3.3 Soot volume fraction distribution.

This section discusses the effects of aromatic fuel addition to *n*-dodecane and premixing on the 2-D distribution of soot. Figure 5 shows the 2-D f_v obtained using LII for the five fuels. The *n*-dodecane flame, shown in Fig. 5(a), is on a scale of 8 ppm, while the four aromatic flames, shown in Fig. 5 (b)-(e), are on a scale of 18 ppm. An iso-contour of 1 ppm is shown on each of the five figures to compare the spatial extent of the f_v. Figs. 5 and 6 show banding of the LII images since each 2-D LII image is compiled by stitching three or four flame images at different HAB; variation in the laser intensity across the laser sheet also contributes to banding in the images. A comparison of Fig. 5 (a) with Fig. 5 (b)-(e) shows that the 2-D structure of f_v for the four aromatic fuels is similar, but is substantially different to that of the *n*-dodecane flame.

In the four aromatic fuels, shown in Fig. 5 (b)-(e), the first location of detection of LII signal in both the annular region and along the centerline is quite similar. Here, the LII signal is first detected at approximately 6 mm HAB as compared to 12 mm HAB for the *n*-dodecane flame. The earlier detection of LII signal in the aromatic flames is expected, as addition of an aromatic fuel to *n*-dodecane results in earlier formation of large aromatics, as discussed in Section 3.2, which would result in soot inception at lower HAB. The first detection of LII signal at similar HAB for the four aromatic fuels is consistent with the large aromatics-LIF results. The LIF signal from large aromatics is also first detected at similar HAB for the four aromatic fuels. Furthermore, the four aromatic flames emit smoke, *i.e,* the soot produced is not oxidized completely. This could be because peak f_v in the aromatic flames is higher, by a factor of 2.6-3.9, as compared to the *n*-dodecane flame. In co-flow ethylene diffusion flames [29], the peak centerline temperature decreased by approximately 150 K due to the increase in peak f_v from 6 ppm to 18 ppm. In the current study, the higher peak f_v in the aromatic flames likely lowers the local flame temperature due to soot radiation cooling, thereby reducing the soot oxidation rate [24].

Numerical simulation of fuel pyrolysis in a homogeneous reactor at a constant temperature of 1600 K using aromatic fuels chemistry from Malewicki *et al*. [30] is conducted in order to identify chemical effects of the five fuels on the key species involved in the soot formation processes. The results from the homogeneous reactor are not meant to directly simulate the flames. Since we wanted to stay as consistent as possible in analyzing the chemistry across the test fuels, we were looking for a single mechanism that had chemistry for *n*-dodecane, *n*-propylbenzene, toluene, *m*-

xylene, and 1,3,5-trimethylbenzene. Malewicki *et al*. [30] is the only mechanism that has all five fuels and therefore, we have used this mechanism. Fig. 7 shows that the peak acetylene concentration is higher in the *n*-dodecane flame than for the four aromatic fuels. Therefore, the increase in the peak f_v in aromatic fuels as compared to *n*-dodecane is most likely due to an increase in aromatic species, as discussed in Section 3.2, which would result in increase in soot inception and soot growth due to PAH condensation.

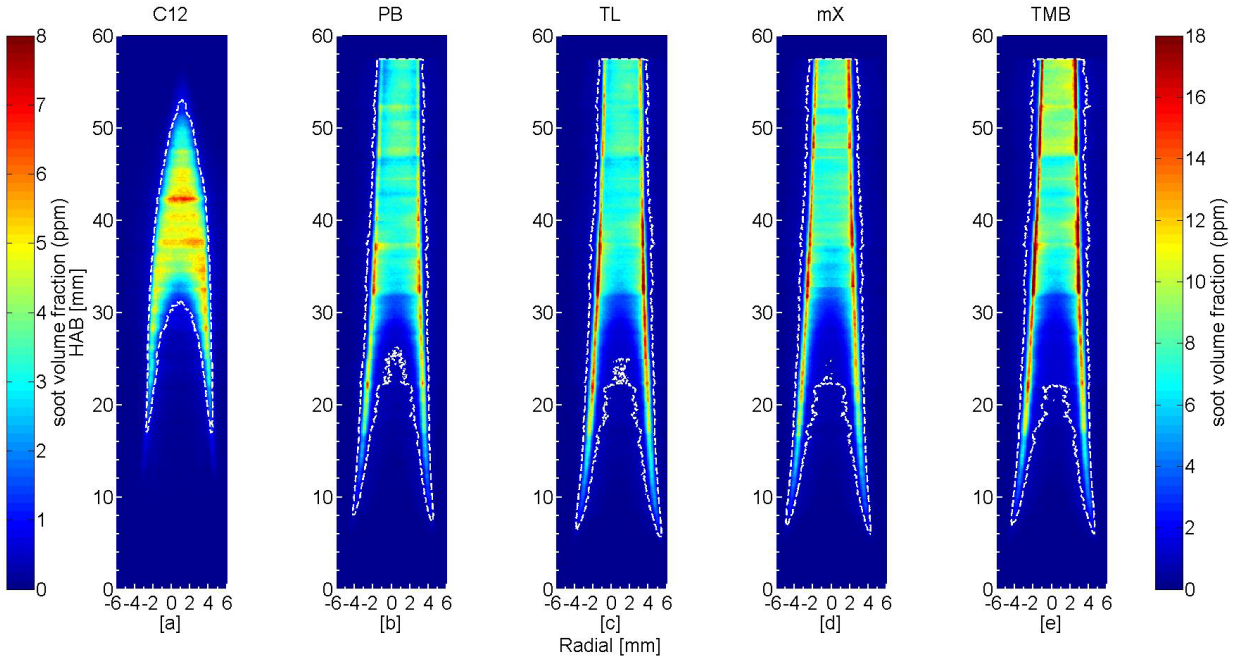

Figure 5. Two dimensional LII image for f_v [ppm] for ϕ_{jet} = Inf: (a) *n*-dodecane flame; (b) *n*-propylbenzene flame; (c) toluene flame; (d) *m*-xylene flame; (e) 1,3,5-trimethylbenzene flame. Note scale of *n*-dodecane is on left while for the four aromatic fuels scale is on right. The dotted line is an iso-contour of 1 ppm.

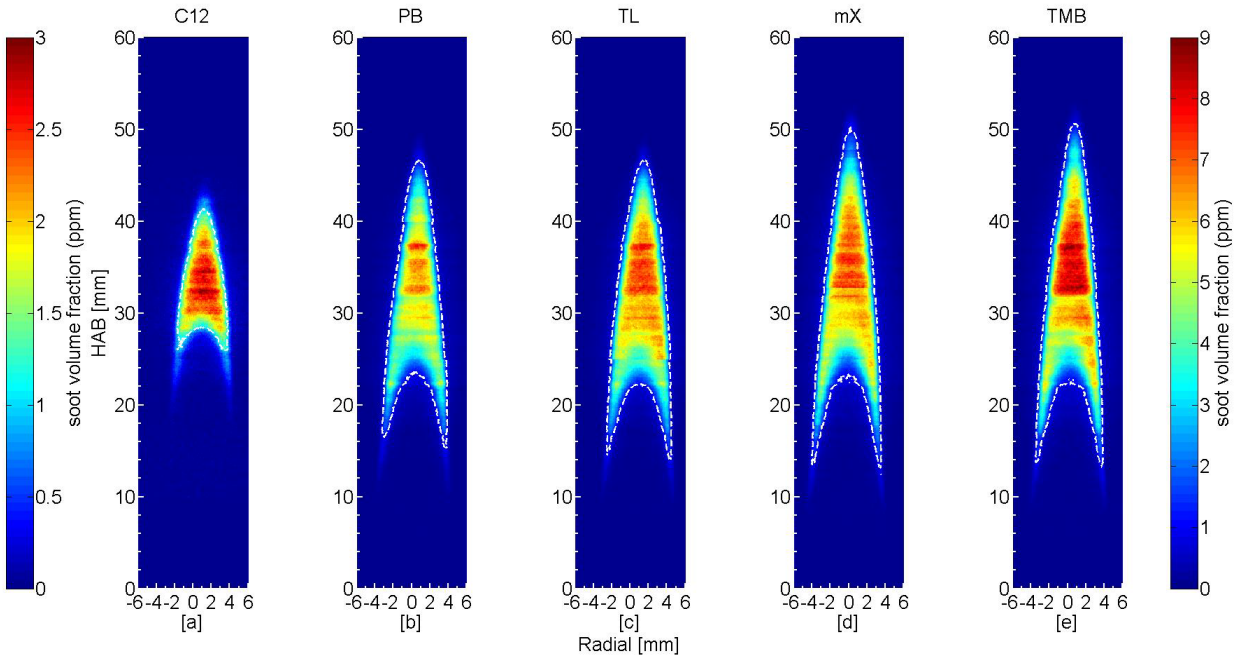

Figure 6. Two dimensional LII image for f_v [ppm] for $\phi_{jet} = 6$: (a) *n*-dodecane flame; (b) *n*-propylbenzene flame; (c) toluene flame; (d) *m*-xylene flame; (e) 1,3,5-trimethylbenzene flame. Note scale of *n*-dodecane is on left while for the four aromatic fuels scale is on right. The dotted line is an iso-contour of 1 ppm.

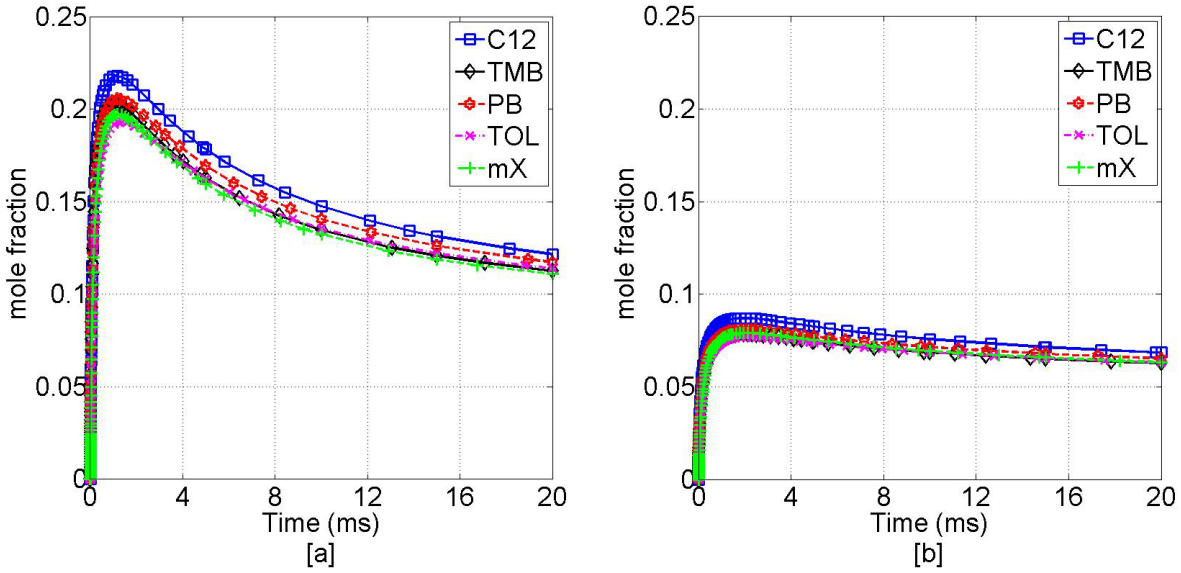

Figure 7. Comparison of acetylene mole fraction for the four aromatic fuel mixtures in a homogeneous reactor at constant temperature (1600 K) and pressure (1 atm) (a) non-premixed condition; (b) partially-premixed condition (ϕ_{jet} =6).

Additionally, Fig. 5 shows that for the *n*-dodecane flame, the peak f_v has a similar magnitude in the annular region and as on centerline. However, for aromatic fuels, the peak f_v at each HAB occurs in a narrow annular region. The peak f_v is higher in the annular region by approximately a factor of two as compared to the peak f_v on the centerline, which indicates that aromatic chemistry tends to have a greater influence on soot in the annular region as compared to the centerline. The higher percentage increase of peak f_v in the annular region as compared to the centerline could be due to enhanced aromatics production as well as higher temperature in the annular region.

Figure 6 shows the 2-D spatial f_v at the $\phi_{jet} = 6$ condition. The *n*-dodecane result is on a scale of 3 ppm, while the aromatic flame results are on a scale of 9 ppm. The addition of air to the fuel jet substantially changes the soot field for the aromatic fuels. In contrast to the non-premixed flames, the premixed aromatic flames do not emit soot. Additionally, the *n*-dodecane and aromatic fuel flames have similar f_v distributions; the soot field is more uniform across the cross-section with the peak f_v location closer to the centerline. Similar to the non-premixed cases, LII signal is first detected at lower HAB in the aromatic flames as compared to the *n*-dodecane flame. Furthermore, the aromatic fuels have a larger spatial extent of LII, from approximately 10 to 50 mm HAB as compared to 18 to 45 mm HAB in the *n*-dodecane flame. The large spatial extent of LII in the aromatic flames is likely a result of earlier formation of soot in aromatic fuels, spurred by accelerated growth of aromatic species. Subsequently, the large peak f_v in aromatic fuel flames needs more time, or height, for soot oxidation. The peak f_v in aromatic fuels is a factor of 2.4-3.0 higher as compared to the *n*-dodecane flame.

The comparison of the f_v spatial distribution for aromatic fuels in Fig. 5 and Fig. 6 shows that the addition of air to fuel causes the peak f_v location to shift from the annular region in the non-premixed flames to a more uniform distribution near the centerline in the $\phi_{jet} = 6$ flames. This shift in peak f_v location with premixing is identical to the trend in the location of the peak large aromatics LIF signal, observed in Fig. 3 and Fig. 4. In the non-premixed flames, Fig. 3 (b)-(e) shows that the peak LIF signal is located in the annular region at 6-20 mm HAB, while in $\phi_{jet} = 6$ flames, Fig. 4 (d) shows that the peak LIF signal is located closer to the centerline at 20-25 mm HAB. It is likely that the transition of peak LIF signal from annular to centerline due to premixing results in an increase in soot inception and soot growth due to PAH condensation on the centerline as compared to the annular region. As a result, the peak f_v location transitions from the annular region to the centerline. A transition of peak f_v location from the annular region to the flame centerline has also

been reported in ethylene flames [24, 29]. In ethylene flames, Smooke *et al*. [29] observed the peak f_v location shifted from the centerline to the annular region with decreasing nitrogen dilution of the fuel jet. Numerical simulation of the flames by the same authors show that the change in the soot field is due to the increase in soot residence time in the annular region and variations in the relative importance of soot inception and growth processes. In the current work, the transition behavior of the soot field is observed due to the addition of air, which has both the chemical/dilution effects of oxygen and the dilution effects of nitrogen.

3.4 Effect of fuel structure and premixing on peak soot volume fraction.

Figure 8 shows the comparison of peak f_v in the whole domain for the five fuels and on the centerline for three ϕ_{jet} at two nitrogen (N_2) flow rates, 0.2 slpm and 0.48 slpm. The data for peak f_v is not reported for *n*-dodecane, 0.48N_2 flames since they were not studied in the previous program [22, 23]. The 95% confidence interval (CI) for the peak f_v in the annular region of the smoking flame, discussed in Appendix G of the Supplemental Material, is ±15%, while the 95% CI for the peak f_v in non-smoking flames and peak f_v on centerline of smoking flames is ±4%.

In the current study, the fuel jet dilution level is increased from standard burner operation at 0.2 slpm to 0.48 slpm N_2 flow rate for the four aromatic fuels. The 0.48 slpm N_2 dilution level was selected to be consistent with our previous work involving the *m*-xylene/*n*-dodecane fuel [22, 23], in which 0.48 slpm N_2 flow rate resulted in a non-smoking flame for the *m*-xylene/*n*-dodecane fuel. At 0.48 slpm N_2 flow rate, all non-premixed and premixed aromatic fuel flames except the 1,3,5-trimethylbenzene/*n*-dodecane, non-premixed flame have a closed tip *i.e.*, all soot that is produced is oxidized. The soot emission in the 1,3,5-trimethylbenzene/*n*-dodecane flame could be a result of higher peak f_v produced in the 1,3,5-trimethylbenzene/*n*-dodecane flame as compared to other aromatic fuels, as is evident in Fig. 8.

Figure 8 (a) shows that the *n*-propylbenzene/*n*-dodecane, toluene/*n*-dodecane, and *m*-xylene/*n*-dodecane fuels, within the measurement uncertainty, have similar peak f_v except at the ϕ_{jet}=Inf-0.2N_2 condition; at this condition, the toluene/*n*-dodecane flame shows higher peak f_v as compared to the *m*-xylene/*n*-dodecane flame. Furthermore, the 1,3,5-trimethylbenzene/*n*-dodecane flame has a higher peak f_v as compared to the *n*-propylbenzene/*n*-dodecane, toluene/*n*-dodecane, and *m*-xylene/*n*-dodecane flames at all six flame conditions. In the smoking flames, the peak f_v is located in a narrow annular region of 0.5 mm at each HAB. Due to a high gradient of f_v in this 0.5 mm, the

95% confidence interval of the LII measurement is greater in the annular region as compared to the centerline. This higher measurement uncertainty in the annular region of smoking flames may be a reason for differences in peak f_v in the toluene/*n*-dodecane and *m*-xylene/*n*-dodecane flame at the ϕ_{jet}=Inf-0.2N2 condition, which is not evident in the non-smoking flames.

In addition, Fig. 8 (b) shows that on centerline, the peak f_v is similar in the *n*-propylbenzene/*n*-dodecane, toluene/*n*-dodecane, and *m*-xylene/*n*-dodecane flames for all six flame conditions. 1,3,5-trimethylbenzene/*n*-dodecane flames produce higher peak f_v as compared to the other three aromatic fuels. However at the two premixing levels of the fuel jet, the differences in the peak f_v among the aromatic flames, at a given ϕ_{jet}, are small in comparison to the resolution of the experiment. To the best of the authors' knowledge, this effect of premixing on f_v for these aromatic fuels has not been reported earlier, and therefore, provides a new dataset to test chemical models for four aromatic fuels under different levels of dilution, at both non-premixed and partially-premixed conditions.

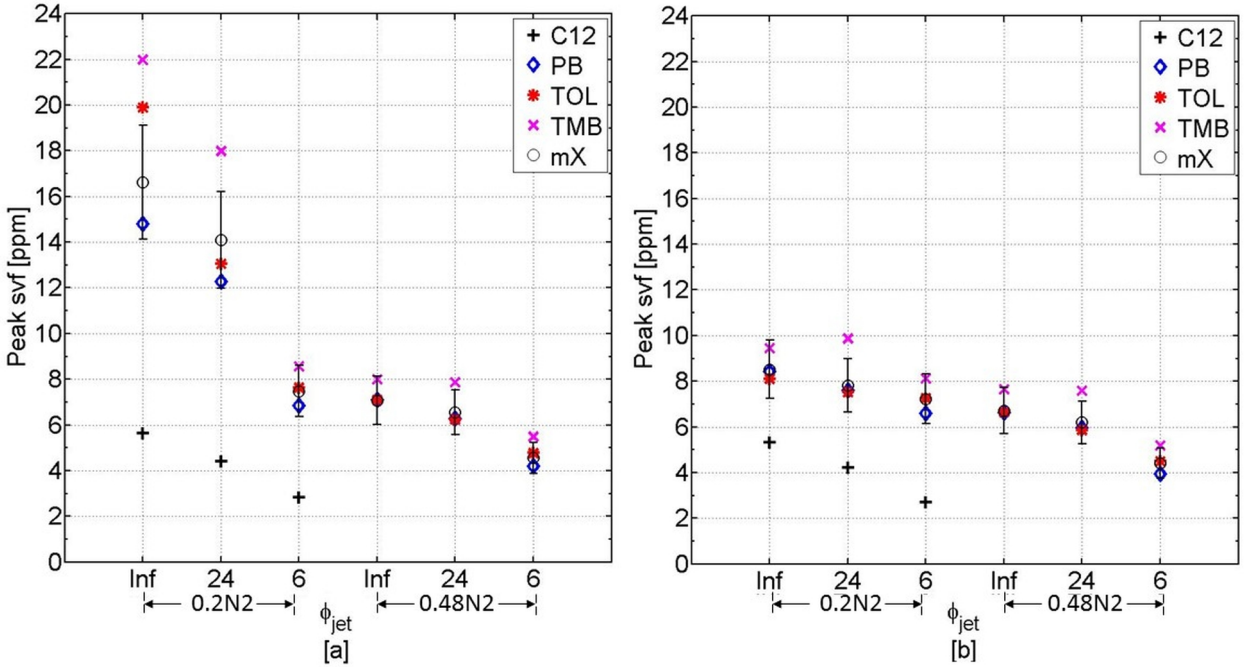

Figure 8. Effect of fuel structure on peak f_v [ppm] in (a) whole domain; (b) centerline. Error bars show ±15% measurement uncertainty.

The relative sooting tendency of the four aromatic fuels is different in the present study as compared to the YSI values reported in McEnally and Pfefferle [31]. The differences in the sooting tendency of the aromatic fuels between YSI and present study could be a result of differences in

the chemistry in the two studies. In YSI, the aromatic fuels react in the chemical and thermal fields of a methane flame, while in the current study, the chemical and thermal fields are from a *n*-dodecane flame. We suspect that the differences in the chemistry of methane and *n*-dodecane flames create differences in the local flame conditions, particularly species, which can impact soot formation processes. Additionally, in YSI, small dopant levels are added to the methane flame, while in the current work, nearly 25% by volume of the fuel comes from the aromatics; therefore, the second fuel can significantly impact the local flame conditions. Conturso *et al*. [7] has also reported differences in the sooting tendency of ethylene/aromatic fuel mixtures and YSI values.

Numerical simulation of fuel pyrolysis, using the chemical mechanism from Malewicki *et al*. [30] in a homogeneous reactor at constant temperature and pressure, is used to compare the pyrene mole fraction amongst the four aromatic fuel mixtures. The pyrene mole fraction is compared because pyrene dimerization is used as the nucleation reaction in several soot models [42, 43]. The simulations are performed at constant temperature to isolate the chemical effects of the initial fuel mixture on the pyrene mole fraction. These simulations in Fig. 9 (a) show that the pyrene mole fraction is similar for the *n*-propylbenzene/*n*-dodecane, toluene/*n*-dodecane, and *m*-xylene/*n*-dodecane fuels, while the pyrene mole fraction is considerably higher in the 1,3,5-trimethylbenzene/*n*-dodecane fuel.

The reaction pathway analysis, shown in Appendix E of the Supplementary Material, shows that higher pyrene in the 1,3,5-trimethylbenzene/*n*-dodecane fuel is a result of higher methylanthracene ($A3CH_3$); $A3CH_3$ can form from DIMERS196 (1-(phenylmethyl)-3,5-dimethylbenzene) through the pathway described in Gudiyella *et al*. [38]. Here, DIMERS196 can form from the reaction of the 1,3,5-trimethylbenzyl radical and benzene, followed by H atom removal. Figure 9 shows that the trend in pyrene mole fraction amongst the four aromatic fuels is consistent under both non-premixed and premixed conditions, ϕ_{jet} =6. Furthermore, comparison of

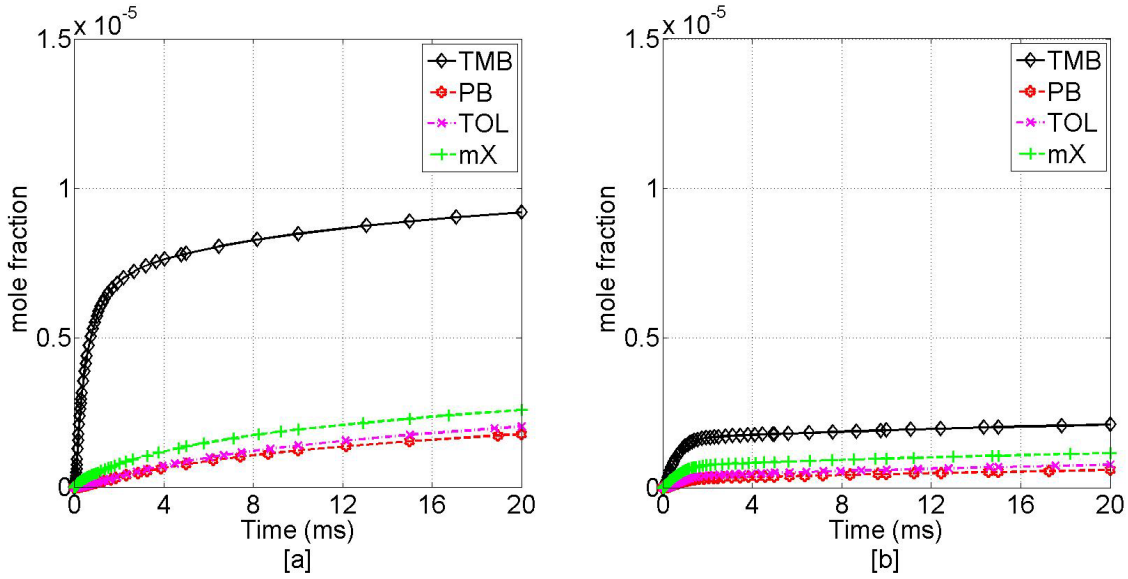

Figure 9. Comparison of pyrene (A4) mole fraction for the four aromatic fuel mixtures in a homogeneous reactor at constant temperature (1600 K) and pressure (1 atm) (a) non-premixed condition; (b) partially-premixed condition (ϕ_{jet} =6).

the pyrene mole fraction in Fig. 9 (a) and (b) shows that the peak concentration of pyrene decreases with premixing, which would result in a decrease in soot nucleation rate.

For the four aromatic fuels, Fig. 8 (a) shows that premixing the fuel jet tends to reduce the peak f_v at both nitrogen flow rates. The percentage reduction in the peak f_v in the $0.2N_2$ and $0.48N_2$ flames is approximately 55-60% and 30-40%, respectively. The reduction in the peak f_v with premixing can be due to a combination of chemical, dilution, and residence time effects, as identified in previous studies [13, 44, 45]; we have discussed these effects in detail in Ref. [23].

4 Conclusions

The current study experimentally investigates the effects of aromatic fuel molecular structure on soot precursors and soot under non-premixed and partially-premixed conditions. The flames are designed such that the temperature in the fuel pyrolysis region at each ϕ_{jet} is similar for the *n*-dodecane and aromatic fuels so as to isolate the chemical effect of the fuels. The results show that under non-premixed conditions, the addition of aromatic fuel to *n*-dodecane results in substantial changes in the 2-D distribution of soot. The comparison of the four aromatic flames with *n*-dodecane shows that aromatic chemistry tends to have a larger effect on the production of soot in the flame annular region as compared to the centerline. As a result, the f_v peaks in a narrow annular

region in the aromatic flames as compared to a uniform soot distribution across the cross-section in the *n*-dodecane flame. At the $\phi_{jet} = 6$ condition, the aromatic fuels and *n*-dodecane have a similar distribution of soot; however, the peak soot volume fraction and spatial extent of the LII signal is greater in the aromatic flames as compared to the *n*-dodecane flame.

The comparison of the four aromatic fuels indicates that at a particular ϕ_{jet}, the location of first detection of large aromatics LIF signal, and hence, LII signal, is found be at similar heights above the tube exit. Quantitatively, LII results show that the *n*-propylbenzene/*n*-dodecane, toluene/*n*-dodecane, and *m*-xylene/*n*-dodecane flames, within measurement uncertainty, produce similar levels of peak soot, while 1,3,5-trimethylbenzene/*n*-dodecane produces a higher level of peak soot. Furthermore, the relative trend of peak soot amongst the four aromatic fuels is found to be the same for both non-premixed (ϕ_{jet} = Inf) and rich-premixed (ϕ_{jet} = 24 and 6) conditions. A published aromatics chemistry is used to understand the differences in the pathway to soot precursors for the four aromatic fuels. The 2-D LIF-LII and temperature measurements provide a new dataset to validate chemical kinetic and soot models for four aromatic fuels, which are important hydrocarbons to represent the aromatic fuel component in surrogate fuels, under both non-premixed and partially-premixed conditions.

5 Acknowledgement

The authors acknowledge the support of the Strategic Environmental Research and Development Program (WP-2145) under the direction of Dr. Robin Nissan and Mr. Bruce Sartwell.

6 References

[1] J.T. Edwards. Reference Jet Fuels for Combustion Testing, 55th AIAA Aerospace Sciences Meeting (2017), AIAA 2017-0146

[2] J. Farrell, N. Cernansky, F. Dryer, C. Law, D. Friend, C. Hergart, R. McDavid, A. Patel, C.J. Mueller, H. Pitsch, Development of an experimental database and kinetic models for surrogate diesel fuels, SAE Technical Paper (2007), 2007-01-0201.

[3] W.J. Pitz, N.P. Cernansky, F.L. Dryer, F. Egolfopoulos, J. Farrell, D. Friend, H. Pitsch, Development of an experimental database and chemical kinetic models for surrogate gasoline fuels, SAE Technical Paper (2007), 2007-01-0175.

[4] H. Richter, J.B. Howard, Formation of polycyclic aromatic hydrocarbons and their growth to soot—a review of chemical reaction pathways, Prog. Energy and Combust. Sci. 26 (2000) 565-608.

[5] T. Zhang, L. Zhao, M.J. Thomson, Effects of n-propylbenzene addition to n-dodecane on soot formation and aggregate structure in a laminar coflow diffusion flame, Proc. Combust. Inst. (2016) 1339-1347.

[6] J. Moss, I. Aksit, Modelling soot formation in a laminar diffusion flame burning a surrogate kerosene fuel, Proc. Combust. Inst. (2007) 3139-3146.

[7] M. Conturso, M. Sirignano, A. D'Anna, Effect of C 9 H 12 alkylbenzenes on particle formation in diffusion flames: An experimental study, Fuel 191 (2017) 204-211.

[8] M. Conturso, M. Sirignano, A. D'Anna, Effect of alkylated aromatics on particle formation in diffusion flames: An experimental study, Exp. Therm and Fluid Sci. 73 (2016) 27-32.

[9] C.S. McEnally, L.D. Pfefferle, Sooting tendencies of nonvolatile aromatic hydrocarbons, Proc. Combust. Inst. 32 (2009) 673-679.

[10] H. Anderson, C.S. McEnally, L.D. Pfefferle, Experimental study of naphthalene formation pathways in non-premixed methane flames doped with alkylbenzenes, Proc. Combust. Inst. 28 (2000) 2577-2583.

[11] S.J. Harris, A.M. Weiner, Soot particle growth in premixed toluene/ethylene flames, Combust. Sci. Technol. 38 (1984) 75-87.

[12] A. D'Anna, M. Alfe, B. Apicella, A. Tregrossi, A. Ciajolo, Effect of fuel/air ratio and aromaticity on sooting behavior of premixed heptane flames, Energy & Fuels 21 (2007) 2655-2662.

[13] C.S. McEnally, L.D. Pfefferle, The effects of slight premixing on fuel decomposition and hydrocarbon growth in benzene-doped methane nonpremixed flames, Combust. Flame 129 (2002) 305-323.

[14] C.P. Arana, M. Pontoni, S. Sen, I.K. Puri, Field measurements of soot volume fractions in laminar partially premixed coflow ethylene/air flames, Combust. Flame 138 (2004) 362-372.

[15] B. Zhao, Z. Yang, Z. Li, M.V. Johnston, H. Wang, Particle size distribution function of incipient soot in laminar premixed ethylene flames: effect of flame temperature, Proceedings of the Combustion Institute 30 (2005) 1441-1448.

[16] C.S. McEnally, L.D. Pfefferle, The effects of premixing on soot production in nonpremixed flames fueled with unsaturated hydrocarbons, Proc. Combust. Inst. 29 (2002) 2407-2413.

[17] S. Dooley, S.H. Won, M. Chaos, J. Heyne, Y. Ju, F.L. Dryer, K. Kumar, C.-J. Sung, H. Wang, M.A. Oehlschlaeger, A jet fuel surrogate formulated by real fuel properties, Combust. Flame 157 (2010) 2333-2339.

[18] M. Colket, T. Edwards, S. Williams, N.P. Cernansky, D.L. Miller, F. Egolfopoulos, P. Lindstedt, K. Seshadri, F.L. Dryer, C.K. Law. Development of an experimental database and kinetic models for surrogate jet fuels. 45th AIAA Aerospace Sciences Meeting and Exhibit (2007), AIAA 2007-770.

[19] A. Agosta, N. Cernansky, D. Miller, T. Faravelli, E. Ranzi, Reference components of jet fuels: kinetic modeling and experimental results, Exp. Therm and Fluid Sci. 28 (2004) 701-708.

[20] P. Dagaut, A. El Bakali, A. Ristori, The combustion of kerosene: Experimental results and kinetic modelling using 1-to 3-component surrogate model fuels, Fuel 85 (2006) 944-956.

[21] J.S. Heyne, M.B. Colket, M. Gupta, A. Jardines, J.P. Moder, J.T. Edwards, M. Roquemore, C. Li, M. Rumizen. Year 2 of the National Jet Fuels Combustion Program: Towards a Streamlined Alternative Jet Fuels Certification Process. 55th AIAA Aerospace Sciences Meeting (2017), AIAA 2017-0145.

[22] Y. Wang, A. Makwana, S. Iyer, M. Linevsky, R.J. Santoro, T.A. Litzinger, J. O'Connor, Effect of fuel composition on soot and aromatic species distributions in laminar, co-flow flames. Part 1. Non-premixed fuel, Combust. Flame, (2017). https://doi.org/10.1016/j.combustflame.2017.08.011

[23] A. Makwana, Y. Wang, S. Iyer, M. Linevsky, R.J. Santoro, T.A. Litzinger, J. O'Connor, Effect of fuel composition on soot and aromatic species distributions in laminar, co-flow flames. Part 2. Partially-premixed fuel, Combust. Flame, (2017). https://doi.org/10.1016/j.combustflame.2017.08.015

[24] R. Santoro, H. Semerjian, R. Dobbins, Soot particle measurements in diffusion flames, Combust. Flame 51 (1983) 203-218.

[25] A. Mouis, A. Menon, V. Katta, T. Litzinger, M. Linevsky, R. Santoro, S. Zeppieri, M. Colket, W. Roquemore, Effects of m-xylene on aromatics and soot in laminar, N 2-diluted ethylene co-flow diffusion flames from 1 to 5atm, Combust. Flame 159 (2012) 3168-3178.

[26] C.R. Shaddix, K.C. Smyth, Laser-induced incandescence measurements of soot production in steady and flickering methane, propane, and ethylene diffusion flames, Combust. Flame 107 (1996) 418-452.

[27] K.C. Smyth, C.R. Shaddix, The elusive history of m~= 1.57–0.56 i for the refractive index of soot, Combust. Flame 107 (1996) 314-320.

[28] T. Edwards, Advancements in gas turbine fuels from 1943 to 2005, J. Eng. Gas Turbines and Power 129 (2007) 13-20.

[29] M. Smooke, R. Hall, M. Colket, J. Fielding, M. Long, C. McEnally, L. Pfefferle, Investigation of the transition from lightly sooting towards heavily sooting co-flow ethylene diffusion flames, Combust. Theory Modelling 8 (2004) 593-606.

[30] T. Malewicki, S. Gudiyella, K. Brezinsky, Experimental and modeling study on the oxidation of Jet A and the n-dodecane/iso-octane/n-propylbenzene/1, 3, 5-trimethylbenzene surrogate fuel, Combust. Flame 160 (2013) 17-30.

[31] C.S. McEnally, L.D. Pfefferle, Improved sooting tendency measurements for aromatic hydrocarbons and their implications for naphthalene formation pathways, Combust. Flame 148 (2007) 210-222.

[32] M. Suto, X. Wang, J. Shan, L. Lee, Quantitative photoabsorption and fluorescence spectroscopy of benzene, naphthalene, and some derivatives at 106–295 nm, J. Quant. Spectrosc. Radiat. Transfer 48 (1992) 79-89.

[33] I. Berlman, Handbook of florescence spectra of aromatic molecules, Elsevier 2012.

[34] J. Emdee, K. Brezinsky, I. Glassman, High-temperature oxidation mechanisms of m-and p-xylene, J. Phys. Chem. 95 (1991) 1626-1635.

[35] S. Gudiyella, T. Malewicki, A. Comandini, K. Brezinsky, High pressure study of m-xylene oxidation, Combust. Flame 158 (2011) 687-704.

[36] P. Dagaut, A. Ristori, A. El Bakali, M. Cathonnet, Experimental and kinetic modeling study of the oxidation of n-propylbenzene, Fuel 81 (2002) 173-184.

[37] W. Yuan, Y. Li, P. Dagaut, Y. Wang, Z. Wang, F. Qi, A comprehensive experimental and kinetic modeling study of n-propylbenzene combustion, Combust. Flame 186 (2017) 178-192.

[38] S. Gudiyella, K. Brezinsky, High pressure study of 1, 3, 5-trimethylbenzene oxidation, Combust. Flame 159 (2012) 3264-3285.

[39] P. Diévart, H.H. Kim, S.H. Won, Y. Ju, F.L. Dryer, S. Dooley, W. Wang, M.A. Oehlschlaeger, The combustion properties of 1, 3, 5-trimethylbenzene and a kinetic model, Fuel 109 (2013) 125-136.

[40] W. Metcalfe, S. Dooley, F. Dryer, Comprehensive detailed chemical kinetic modeling study of toluene oxidation, Energy Fuels 25 (2011) 4915-4936.

[41] W. Yuan, Y. Li, P. Dagaut, J. Yang, F. Qi, Investigation on the pyrolysis and oxidation of toluene over a wide range conditions. II. A comprehensive kinetic modeling study, Combust. Flame 162 (2015) 22-40.

[42] A. Veshkini, S.B. Dworkin, M.J. Thomson, A soot particle surface reactivity model applied to a wide range of laminar ethylene/air flames, Combust. Flame 161 (2014) 3191-3200.

[43] A. Khosousi, S.B. Dworkin, Detailed modelling of soot oxidation by O 2 and OH in laminar diffusion flames, Proc. Combust. Inst. 35 (2015) 1903-1910.

[44] Ö.L. Gülder, Effects of oxygen on soot formation in methane, propane, and n-butane diffusion flames, Combust. Flame 101 (1995) 302-310.

[45] I. Glassman. Sooting laminar diffusion flames: effect of dilution, additives, pressure, and microgravity, Symp. (Int.) Combust. 27 (1998) p. 1589-1596.